

PERFORMANCE STUDIES OF INDUSTRIAL CCD CAMERAS BASED ON SIGNAL-TO-NOISE AND PHOTON TRANSFER MEASUREMENTS

G. Kube, DESY, Hamburg, Germany

Abstract

Area scan sensors are widely used for beam profile measurements in particle beam diagnostics. They provide the full two-dimensional information about the beam distribution, allowing in principle to investigate shot-to-shot profile fluctuations at moderate repetition rates. In order to study the performance and to characterize these cameras, photon transfer is a widely applied popular and valuable testing methodology. In this report, studies based on signal-to-noise and photon transfer measurements are presented for CCD cameras which are in use for beam profile diagnostics at different DESY accelerators.

INTRODUCTION

Area scan CCD or CMOS sensors are widely used in beam diagnostics because they provide the full two-dimensional information about the transverse particle beam distribution. For this purpose the information about the particle beam charge distribution is converted in an optical intensity distribution which is recorded by the area scan detector. This light distribution can either be generated in an interaction of the particle beam with material, resulting in atomic excitations which are followed by radiative relaxations (e.g. in scintillating screen or beam induced fluorescence monitors [1, 2]). Alternatively, light extracted from the electromagnetic fields accompanying an ultra-relativistic particle beam can be utilized as it is the case e.g. for synchrotron, transition or diffraction radiation based monitors [3].

For high resolution beam profile measurements, care has to be taken that any resolution broadening introduced by the basic underlying physical process and/or the optical system has to be small. In addition, the conversion process from the charged particle distribution in digital numbers in the data acquisition system has to be linear to avoid any misinterpretation of measured beam sizes and shapes. The linearity may be distorted either by the generation of the photon intensity distribution (e.g. by saturation effects in scintillators or microbunching instabilities in high-brightness electron beams [4]), or in the conversion from a photon distribution into a set of digital numbers in the camera.

The objective of the present study is to focus on the last aspect and to characterize the quality of area scan cameras which are in use for beam profile diagnostics. While there is no principal difference in the characterization between CCD and CMOS sensors, in the following only industrial CCD cameras are considered which are in use at different DESY accelerators. The sensor characterization is based on the Photon Transfer (PT) method which is a valuable methodology employed for solid state imager and camera system investigations. In the next section the PT basic principle is

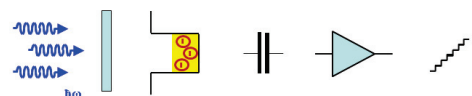
introduced and it is demonstrated how sensor parameters can be derived from Signal-to-Noise Ratio (SNR) measurements. Afterwards, the laboratory setup together with CCD performance measurements is presented.

PRINCIPLE OF CHARACTERIZATION

PT is widely used for image sensor testing because it is a straightforward method to determine numerous sensor parameters by analyzing only two measured quantities, average signal and rms noise. Detailed information about PT can be found in textbooks (e.g. Ref. [5]), and the European Machine Vision Association even derived the EMVA Standard 1288 according to this method [6]. Following this standard a brief introduction in the underlying mathematical model is given in this section. According to Ref. [6] this model is valid if (i) the amount of photons collected by a pixel depends on the radiative energy density, (ii) noise sources are stationary and white, (iii) only the total quantum efficiency is wavelength dependent, (iv) only the dark current depends on temperature, and (v) the sensor is linear, i.e. the digital signal y increases linear with the number of photons received. It is interesting to point out that the latter condition imposes a lower limit on the applicable wavelength region because the quantum yield in silicon is larger than one for photon wavelengths smaller than 400 nm [7].

As illustrated in Fig.1(a), the digital image sensor converts photons impinging on the pixel area in a series of steps into a

(a) physical camera model for signal generation



56

(b) mathematical model of single pixel

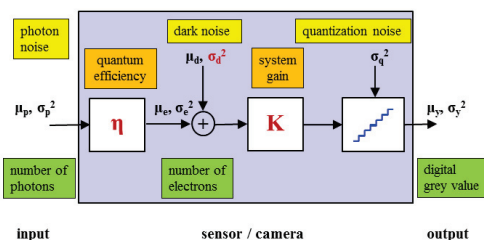


Figure 1: (a) Physical camera model: a number of photons hitting a sensor pixel creates a number of electrons via the photoelectric effect. The resulting charge is converted by a capacitor to a voltage, then amplified and digitized. As result a digital grey value is generated. (b) Mathematical model of a single pixel.

digital number. The number of incoming photons n_p follows a Poisson distribution, due to their statistical fluctuations it is suitable to characterize the process by the mean number of incoming photons μ_p with corresponding variance $\sigma_p^2 = \mu_p$. A fraction of the incoming photons is absorbed and generates photo electrons in the CCD pixel with μ_e the mean number of accumulated charges. A Poisson random process (photon emission with mean μ_p) that is thinned by binomial selection with success probability (quantum efficiency) η is again following a Poisson distribution with mean $\mu_e = \eta\mu_p$ and variance $\sigma_e^2 = \mu_e$, which can be rewritten as $\sigma_e = \sqrt{\eta}\sigma_p$.

In the camera electronics, the accumulated charge is converted into a voltage, amplified and finally transformed to a digital number y , assuming each of these processes to be linear. In the mathematical model shown in Fig.1(b) the individual processes are summarized in a single quantity, the overall system gain K with units Digital Number (DN) per electrons. With μ_d the mean dark electrons, the mean digital signal or grey value μ_y can be written as

$$\mu_y = K(\mu_e + \mu_d) = K\eta\mu_p + \mu_{y,dark} . \quad (1)$$

Here $\mu_{y,dark}$ indicates the mean dark signal $K\mu_d$.

A similar consideration can be performed for the temporal noise which is characterized by its corresponding variance σ_i^2 , where i stands for an arbitrary noise source. The variance of the fluctuations of the accumulated charges σ_e^2 is often referred as shot noise, all other noise sources depend on the specific sensor and camera electronic layout and their variances add up in a linear way due to the linear signal model. Treating the whole camera as a black box as it is indicated in Fig.1(b), it is sufficient to consider only two additional noise sources [6]: the ones related to sensor read out and amplifier circuits, described by a signal independent normal distributed source with variance σ_d^2 , and the final analog-to-digital conversion which is distributed uniformly between the quantization intervals and has a variance $\sigma_q^2 = 1/12 \text{ DN}^2$. According to the laws of error propagation, the total variance σ_y^2 of the digital signal y is given by

$$\sigma_y^2 = K^2(\sigma_d^2 + \sigma_e^2) + \sigma_q^2 , \quad (2)$$

which can be rewritten as

$$\sigma_y^2 = K(\mu_y - \mu_{y,dark}) + \sigma_{y,dark}^2 \quad (3)$$

using Eq. (1) and $\sigma_{y,dark} = K\sigma_y$. Furthermore it is assumed that the contribution of the quantization noise is negligible compared to the dark noise.

Eqn. (1) and (3) are fundamental for the sensor characterization because they represent linear relations for experimentally accessible parameters. According to Eq. (1), a measurement of the mean grey value as function of the mean number of incoming photons delivers ($K\eta$) as slope and $\mu_{y,dark}$ as offset. A measurement of the variance of the grey values as function of the background corrected mean grey value results in K as slope and $\sigma_{y,dark}^2$ as offset according to Eq. (3). As consequence, a number of relevant sensor parameters is accessible from these measurements.

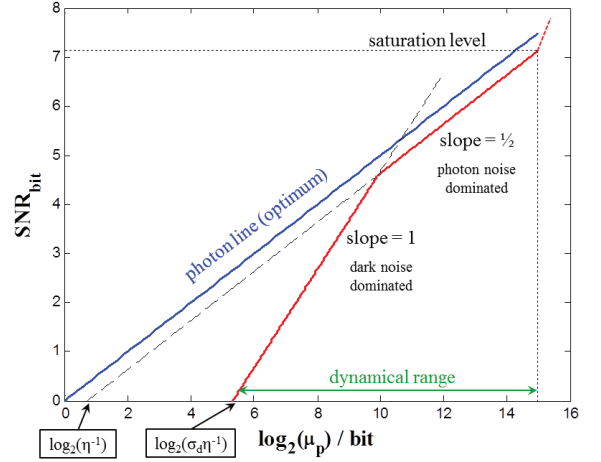


Figure 2: SNR as function of the incoming number of photons for an ideal (blue) and a real (red) sensor. More details see text.

Signal-to-Noise Ratio The quality of a detector signal is usually expressed by the Signal-to-Noise Ratio (SNR), defined by $\text{SNR} = (\mu_y - \mu_{y,dark})/\sigma_y$. Using Eqn. (1), (3) and taking the base 2 logarithm $\log_2(\text{SNR}) = \text{SNR}_{\text{bit}}$, SNR can be rewritten as

$$\text{SNR}_{\text{bit}} = \log_2(\eta) + \log_2(\mu_p) - \frac{1}{2} \log_2(\eta\mu_p + \sigma_d^2) . \quad (4)$$

It is interesting to consider the case of an ideal sensor with quantum efficiency $\eta = 1$ and no noise, i.e. $\sigma_d = 0$. In this situation $\text{SNR}_{\text{bit}} = 1/2 \log_2(\mu_p)$ or $\text{SNR} = \sqrt{\mu_p}$, i.e. SNR represents the pure photon shot noise. It is obvious that a real sensor cannot be better than an ideal sensor. As consequence, in the SNR diagram in Fig.(2) the curve of a real sensor is always below the photon line. Moreover, two limiting cases can be considered:

shot noise dominated: $\eta\mu_p \gg \sigma_d^2$. For high photon intensities the SNR relation Eq. (4) can simply be written as

$$\text{SNR}_{\text{bit}} = \frac{1}{2} \log_2(\mu_p) + \frac{1}{2} \log_2(\eta) . \quad (5)$$

As shown in Fig.(2), in this region the SNR yields a straight line with slope $\frac{1}{2}$ which crosses the x-axis in the point $\log_2(\eta)$, i.e. the minimum detectable number of photons ($\text{SNR} = 1:1$) amounts to η^{-1} , assuming the sensor would have a pure shot noise characteristics.

dark noise dominated: $\eta\mu_p \ll \sigma_d^2$. Unfortunately a real sensor is also affected by the dark noise. For very low photon intensities the SNR relation is transformed into

$$\text{SNR}_{\text{bit}} = \log_2(\mu_p) + \log_2(\eta\sigma_d^{-1}) . \quad (6)$$

If the dark noise dominates the SNR yields a straight line with slope 1, crossing the x-axis in the point $\log_2(\eta\sigma_d^{-1})$. As consequence, the minimum detectable signal ($\text{SNR} = 1:1$) of the real sensor amounts to $\sigma_d\eta^{-1}$.

If the photon intensity is further increased, saturation occurs at a saturation irradiation $\mu_{p,sat}$ which corresponds to

a saturation capacity $\mu_{e,sat} = \eta\mu_{p,sat}$. For a k -bit digital camera, the digital values will then be clipped to the maximum digital grey value $2^k - 1$. According to Ref. [6] the saturation capacity must not be confused with the full-well capacity, it is normally lower because the signal is clipped to the maximum digital value before the physical pixel saturation is reached. As consequence of the signal clipping, the variance σ_y^2 decreases and SNR_{bit} steeply increases. From the minimum detectable signal and the saturation irradiation the dynamical range of the sensor can be deduced as indicated in Fig.(2).

Therefore, also the analysis of the SNR diagram gives access to a number of important sensor parameters. In the next section, the laboratory setup for the camera characterization together with the measurement procedure will shortly be described.

SETUP AND MEASUREMENT

The camera is mounted together with a flat field illumination onto an optical bench in the laboratory, the distance between both is about 720 mm. The camera is operated without objective lens, no obstacles like diffusors or apertures are placed in the light path such that the homogeneity of the illumination is determined directly by the light source itself. During operation, the whole setup is covered with a light shielding in order to avoid stray light contributions.

As light source a flatfield LED illumination (CCS TH-100/100) with peak wavelength $\lambda_p = 470$ nm is used which has a rather good surface homogeneity with variations in the order of about 5% in the central part. However, in order to resolve individual noise contributions as the sensor fixed pattern noise, a homogeneity of better than 1% would be required [5]. The light source irradiance was calibrated with a cw powermeter (Ophir Nova II with PD300-UV detector head), and with knowledge of the CCD exposure time t_{exp} and the pixel area the irradiance can be converted in a number of incoming photons μ_p .

For the measurement of a PT resp. an SNR sequence μ_p has to be varied. This was realized by operating the light source with fixed irradiance and changing t_{exp} . Advantage of this method is that the light source is kept in thermal balance, disadvantage is that for each exposure time a background image for the determination of $\mu_{y,dark}$ has additionally to be taken, because the number of thermally induced electrons contributing to the dark signal linearly depends on t_{exp} [6]. CCD readout was performed based on the TINE AVINE video system [8,9].

In order to have sufficient statistical significance in the measurements, for each t_{exp} a series of 10 images was recorded and the determination of mean μ_y and total variance σ_y^2 of the digital signal was performed in a selected ROI of 50x50 pixel.

ANALYSIS

The measurements were performed for three camera types which are in operation at DESY: (i) Basler Aviator avA1600-

50gm in used at the PETRA III accelerator, (ii) JAI BM-141GE in use at PETRA III, REGAE and PITZ, and (iii) Sony XCG-H280E in use at REGAE. In the following, data are shown only for camera (i). For the remaining cameras, only the derived parameters will be quoted.

Fig.3 shows PT measurements derived for the Basler Aviator avA1600-50gm. Fitting the responsivity curve (a) in a range between minimum intensity and 70% of saturation capacity with a straight line following the recommendation in Ref. [6] results in a slope 0.0802 which corresponds to $K\eta$ according to Eq. (1). Repeating the procedure for the PT curve (b) results in a slope $K = 0.1793$ DN/e⁻ and an offset of $\sigma_{y,dark}^2 = 5.093$ DN² according to Eq. (3).

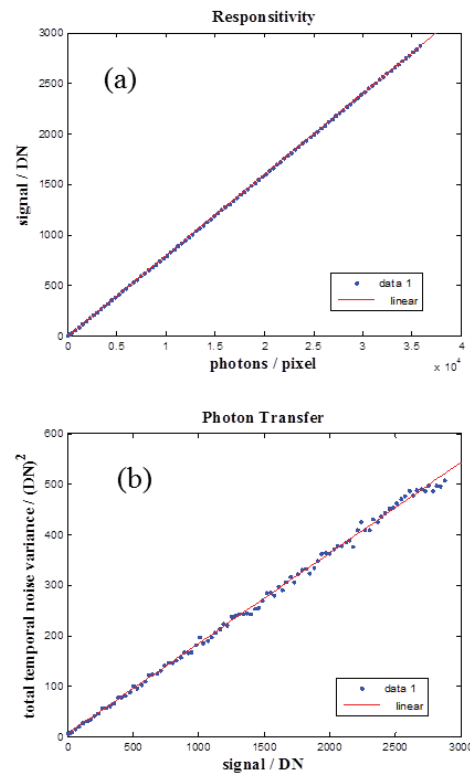


Figure 3: PT curves for the Basler Aviator avA1600-50gm. (a) Responsivity curve according to Eq. (1). (b) PT curve according to Eq. (3). Both curves were fitted with a straight line in a region between minimum intensity and 70% of saturation capacity [6].

In Table 1 the parameters are summarized after combination (column 2) and compared to the the EMVA data sheet (column 4) [10]. Instead of using the overall system gain K the reciprocal parameter is often quoted as indicated in the table. Furthermore, the noise is expressed in units of e⁻ instead of DN which can simply be converted by multiplication with K^{-1} . As one can see from this comparison, the measurement is in satisfactory agreement with the data sheet parameters. Nevertheless there is a larger discrepancy in K^{-1} . The measurement was repeated with different cameras of this type and this discrepancy could be reproduced in each

Table 1: Quantum efficiency η , inverse system gain K^{-1} , and temporal dark noise σ_d , as derived from the PT diagrams (column 2), the SNR analysis (column 3) and taken from the data sheet (column 4). The error in η is estimated to be in the order of 5%, in K^{-1} in the order of 7% and of σ_d in the order of 2%.

item	PT	SNR	data sheet
η	45%	40%	40%
K^{-1}	5.6 e ⁻ /DN	-	4.8 e ⁻ /DN
σ_d	12.6 e ⁻	12.2 e ⁻	11 e ⁻

measurement. Therefore there is a suspicious that the gain in the data sheet is not quoted correctly.

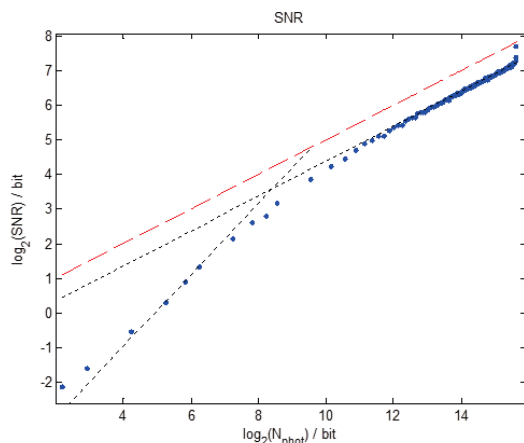


Figure 4: SNR diagram. The photon line is indicated by the red dashed line, the slope 1 and slope $\frac{1}{2}$ interpolations by the black dashed lines.

Fig.4 shows the same data set plotted as SNR diagram. From the intersection points of the slope 1 and slope $\frac{1}{2}$ interpolations, the quantum efficiency and the temporal dark noise σ_d can be deduced. Both parameters which are shown in column 3 of Tab.1 are in good agreement with the PT measurements and the data sheet.

In addition, from the steep increase in the SNR diagram at about 15.52 bit the saturation irradiance can be derived to $\mu_{p,sat} = 2^{15.52} = 46988$ which corresponds to a saturation capacity of $\mu_{e,sat} = 18800e^{-1}$. This value is in excellent agreement with the one from the data sheet [10]. Furthermore, with knowledge of the saturation irradiance and the minimum detectable signal $\mu_{p,min} = \sigma_d/\eta = 30.6$, the dynamical range can be deduced according to $DR = \mu_{p,max}/\mu_{p,min} = 1535$, corresponding to $DR = 10.6$ bit and compared to 10.7 bit as quoted in the data sheet.

SUMMARY

In this report, a method to derive camera sensor parameters independently of manufacturer data sheets is presented which is based on the analysis of PT and SNR diagrams according to Refs. [5, 6]. It is very helpful because not every manufacturer will provide all relevant sensor parameters

which are accessible via these measurements. By application of this method it is possible to compare the camera performance based on a standard set of parameters.

It was shown that the measured parameters of a Basler Aviator avA1600-50gm are in good agreement with the ones from the camera data sheet. The analysis was repeated not only for one but for more cameras of this model type, showing a very good agreement. Moreover, different camera types were under investigation and the results are summarized in Table 2. The Sony XCG-H280E for example shows a very

Table 2: Parameter Comparison for Different CCDs

item	Basler	JAI	Sony
η	42.5%	60%	58%
K^{-1}	5.6 e ⁻ /DN	4.1 e ⁻ /DN	2.0 e ⁻ /DN
σ_d	12.4 e ⁻	15.3 e ⁻	8.8 e ⁻
$\mu_{e,sat}$	18800 e ⁻	16080 e ⁻	6540 e ⁻
DR	10.6 bit	9.3 bit	9.6 bit

high quantum efficiency and dark noise for high sensitivity applications, but also a rather low saturation capacity with acceptable dynamical range. The JAI BM-141GE at the other hand has also a very high η , but with higher noise and better $\mu_{e,sat}$. Depending on the dedicated application, with the knowledge of the relevant sensor parameters a purposeful camera selection can therefore be performed.

ACKNOWLEDGMENT

The author thanks S. Weisse (DESY Zeuthen) for providing the TINE AVINE video server, and H. Delsim-Hashemi (DESY) for making available the access to the JAI and Sony cameras.

REFERENCES

- [1] B. Walasek-Höhne and G. Kube, Proc. DIPAC'11, Hamburg, Germany, May 2011, WEOB01, p.553 (2011).
- [2] P. Forck, Proc. IPAC'10, Kyoto, Japan, May 2010, TUZMH01, p.1261 (2010).
- [3] G. Kube, Proc. IBIC'14, Monterey (CA), USA, September 2014, TUIZB1, p.263 (2014).
- [4] S. Wesch and B. Schmidt, Proc. DIPAC'11, Hamburg, Germany, May 2011, WEOA01, p.539 (2011).
- [5] J.R. Janesick, *Photon Transfer*, (SPIE Press, Bellingham, Washington USA 2007).
- [6] EMVA Standard 1288, Release 3.1, Release Candidate (2012): www.emva.org
- [7] F.J. Wilkinson *et al.*, J. Appl. Phys. **54** (1983) 1172.
- [8] S. Weisse *et al.*, Proc. ICALEPCS'09, Kobe, Japan, October 2009, MOD003, p.34 (2009).
- [9] S. Weisse *et al.*, Proc. ICALEPCS'11, Grenoble, France, October 2011, MOPMS033, p.405 (2011).
- [10] Basler AG – Industrial Camera Manufacturer, www.baslerweb.com